



HAL
open science

Impact of bubble coalescence in the determination of bubble sizes using a pulsed US technique: Part 2 – Effect of the nature of saturating gas

Rachel Pflieger, Geoffrey Audiger, Sergey I. Nikitenko, Muthupandian Ashokkumar

► To cite this version:

Rachel Pflieger, Geoffrey Audiger, Sergey I. Nikitenko, Muthupandian Ashokkumar. Impact of bubble coalescence in the determination of bubble sizes using a pulsed US technique: Part 2 – Effect of the nature of saturating gas. *Ultrasonics Sonochemistry*, 2021, 73, pp.105537. 10.1016/j.ultsonch.2021.105537. cea-03234659

HAL Id: cea-03234659

<https://cea.hal.science/cea-03234659>

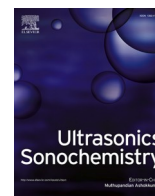
Submitted on 28 May 2021

HAL is a multi-disciplinary open access archive for the deposit and dissemination of scientific research documents, whether they are published or not. The documents may come from teaching and research institutions in France or abroad, or from public or private research centers.

L'archive ouverte pluridisciplinaire **HAL**, est destinée au dépôt et à la diffusion de documents scientifiques de niveau recherche, publiés ou non, émanant des établissements d'enseignement et de recherche français ou étrangers, des laboratoires publics ou privés.



Distributed under a Creative Commons Attribution - NonCommercial - NoDerivatives 4.0 International License



Impact of bubble coalescence in the determination of bubble sizes using a pulsed US technique: Part 2 – Effect of the nature of saturating gas

Rachel Pflieger^{a,*}, Geoffrey Audiger^a, Sergey I. Nikitenko^a, Muthupandian Ashokkumar^b

^a ICSM, Univ Montpellier, CEA, CNRS, ENSCM, Marcoule, France

^b School of Chemistry, University of Melbourne, Melbourne, VIC 3010, Australia

ARTICLE INFO

Keywords:

Bubble size
Pulsed ultrasound
Coalescence
Sonoluminescence
He
Xe
N₂
O₂
Air

ABSTRACT

Knowledge on cavitation bubble size distribution, ambient radius of bubbles is of interest for many applications that include therapeutic and diagnostic medicine. It however becomes a hard quest when increasing the ultrasonic frequency, when direct observation of bubble dynamics is no longer possible. An indirect method based on the estimation of the bubble dissolution time under pulsed ultrasound (362 kHz) is used here under optimized conditions to derive ambient radii of cavitation bubbles in water saturated with He, Ar, Xe, O₂, N₂ and air: 3.0 μm for Ar, 1.2 μm for He, 3.1 μm for Xe, 2.8 μm for O₂, around 1 μm for N₂ and air. If the pulse on-time is increased, bubble coalescence occurs, the extent of which is rather limited for Ar but extremely high for He or N₂.

1. Introduction

Determination of bubble populations and sizes in a cavitation field is of prime importance to optimize sonochemical processes and other ultrasound related applications [1,2]. Among the limited experimental methods available [3–6], only very few allow measurements up to very high US frequencies, i.e., in the range of interest for medical (therapeutic and diagnostics) applications. These indirect methods are based on the correlation between bubble dissolution rate and bubble size. In the first one [3–6], the evolution of the void rate in solution after US irradiation was followed using an electromagnetic method. The second one [7] used an acoustic method to follow the scattering intensity of bubbles vs time. These two methods gave access to a distribution in size of all bubbles in solution, not just to the cavitation bubbles. The third one [8,9] a priori advantageously restricts the focus on sonoluminescing or on sonochemiluminescing bubbles, being based on the measurement of sonoluminescence (SL) or sonochemiluminescence (SCL) intensity under pulsed US conditions. Briefly, by monitoring the evolution of the SL intensity with a decreasing pulse off-time for a constant on-time, the dissolution time of bubbles can be inferred, and from it the corresponding bubble size and size distribution can be determined. Its weaknesses have however been recently underlined [10]. The present study, divided in two parts, aims at a better understanding of the phenomena taking place

under pulsed US and at the determination of conditions in which measurements indeed lead to a cavitation bubble size. The first part [10] focused on Ar-saturated water sonicated at 362 kHz. It has brought to light that great care must be taken in the choice of the pulse on-time (t_{on}) and in the experimental geometry. Indeed, if the on-time is not reduced to a minimum (around 1 ms or less for Ar), coalescence of bubbles takes place and leads to the measurement of the size of coalesced bubbles instead of cavitation bubbles. Longer the on-time, larger is the determined size, because more bubbles are formed during t_{on} , which increases the probability of interaction and coalescence. Besides, the formation of a standing wave should be avoided, since it favors coalescence. In optimized conditions, a bubble size of about 2.9–3.0 μm was estimated for Ar-saturated water sonicated at 362 kHz.

This second part (current manuscript) aims at extrapolating the proposed method to other gases (He, Xe, O₂, N₂) showing very different solubilities and physical properties, and to some chosen gas mixtures (Ar-N₂ with different ratios, air). Pre-saturated water was used, without continuous gas flow, since it was previously [10] shown that the presence of a continuous gas flow favors bubble coalescence.

2. Materials & methods

A detailed description of the set-up and of the method can be found

* Corresponding author.

E-mail address: Rachel.Pflieger@cea.fr (R. Pflieger).

<https://doi.org/10.1016/j.ultsonch.2021.105537>

Received 7 September 2020; Received in revised form 25 February 2021; Accepted 18 March 2021

Available online 22 March 2021

1350-4177/© 2021 The Authors.

Published by Elsevier B.V. This is an open access article under the CC BY-NC-ND license

(<http://creativecommons.org/licenses/by-nc-nd/4.0/>).

in Part I of this study [10]. Water was pre-saturated with the gas of interest (He, Xe, O₂, N₂; 99.999%, Air Liquide) by sparging it in the solution for 30 min. Gas mixtures were prepared in situ using a double entry flowmeter (Aalborg). The acoustic frequency used was 362 kHz and the absorbed acoustic power, determined calorimetrically, was 47 W. The water temperature was kept at 10 °C using a thermocryostat. The on-time was made to vary between 1 and 8 ms, and the off-time, for each t_{on} value, between 200 and 1000 ms (it was checked that the SL intensity was very low below 200 ms). Presented evolutions of the SL intensity during t_{on} were taken at a t_{off} corresponding to the end of the SL intensity increase.

3. Results & discussion

The bubble sizes were measured at an acoustic power of 47 W to avoid standing wave formation. The measurements were also performed at 4.4 W but are not shown here. They confirm that larger sizes are obtained at low acoustic power, similar to the Ar case [10] and that the greater occurrence of coalescence in the standing-wave configuration is not dependent on the nature of the gas.

3.1. Evolution of the SL intensity during t_{on}

The evolution of the SL intensity during t_{on} (taken at a t_{off} corresponding to the end of the SL intensity increase) is presented in Fig. 1 for He, Xe, O₂, N₂ and the gas mixtures air and Ar-N₂ 50–50.

It was previously shown in Ar saturated water that only cases with a continuous increase in SL intensity during t_{on} may correspond to cavitation bubbles. A change in slope indeed indicates interaction between bubbles and in particular formation of coalesced bubbles. In Ar-saturated water, a regular increase was observed for $t_{\text{on}} = 0.5 - 3$ ms.

Different behaviors are observed for the different gases. For He, with $t_{\text{on}} = 1$ ms, the SL intensity increases continuously during 1 ms. Thus there is no indication of pronounced coalescence. The 2 ms case is already different where a first plateau is reached after 1 ms US. Thus bubble sizes determined for $t_{\text{on}} \geq 2$ ms are expected to include sizes of coalesced bubbles. For Xe on the contrary, strong bubble interactions are already detected for $t_{\text{on}} = 1$ ms: SL is increasing during 2 ms but with a change in slope after 0.6 ms. This means that bubble sizes inferred from 1 ms measurements are already expected to include coalesced bubbles. For oxygen, a change in slope is also already observed for $t_{\text{on}} = 1$ ms, indicating interactions between bubbles. For nitrogen, the SL was too dim to allow measurements with $t_{\text{on}} = 1$ ms. For $t_{\text{on}} = 2$ ms, the SL intensity increases continuously during the US irradiation then decreases. For $t_{\text{on}} = 3$ ms a change in slope is observed after ≈ 1.8 ms indicating that corresponding experimental bubble sizes may correspond to coalesced bubbles. In nitrogen-containing gas mixtures (air and Ar 50% - N₂ 50%), coalescence is already observed for $t_{\text{on}} = 1$ ms. In air, the SL intensity increases during 2 ms: it first reaches a plateau after 1 ms then increases again. In Ar 50% - N₂ 50%, a first plateau is reached after 0.8 ms then the SL intensity continues increasing (until almost 1 ms after the end of the US pulse).

It is observed for all gases that for $t_{\text{on}} = 1$ ms SL is emitted during a larger time than the set US pulse. This phenomenon has been (at least partly) attributed to a longer emission of the transducer at very low (≤ 1 ms) on-times (see Fig. 3SI in the Supporting Information of Part I of this study [10]).

3.2. Derived bubble sizes

Bubble sizes were calculated from SL intensity vs. t_{off} plots using the equation of bubble dissolution [16], as previously [9,17] described. They are summarized in Table 1.

For all studied gases and as was previously observed on Ar, an increase in the determined bubble sizes is seen when increasing t_{on} . Its extent depends on the gas nature. For instance, it is very marked for He:

considering the smallest size (1.2 μm) as the ambient radius one gets that a bubble arising from the coalescence of 2 bubbles of radius 1.2 μm will have a radius of $1.2 \times \sqrt[3]{2} = 1.5$ μm . Similarly, the coalescence of 2 bubbles of radius 1.5 μm will give a bubble of 1.9 μm radius ($1.5 \times \sqrt[3]{2} = 1.9$ μm), that of 2 bubbles of radius 1.9 μm a bubble of 2.4 μm radius, that of 2 bubbles of radius 2.4 μm a bubble of radius 3.0 μm and so on. Thus the different values in Table 1 can be explained by bubble coalescence, as was previously discussed for Ar [10]. Owing to He low solubility one may assume that the lowest determined value at 1 ms may be considered as a cavitation bubble size (R_0): 1.2 μm .

With Xe as the saturating gas, as was discussed above, strong bubble interactions are present already for $t_{\text{on}} = 1$ ms and corresponding bubble sizes are expected to be already sizes of coalesced bubbles. The smallest measured size is 4.9 μm . It may arise from the coalescence of:

$$2 \text{ bubbles, leading to a } R_0 \text{ of } 4.9 / \sqrt[3]{32} = 3.9 \mu\text{m}$$

$$3 \text{ bubbles, leading to a } R_0 \text{ of } 4.9 / \sqrt[3]{33} = 3.4 \mu\text{m}$$

$$4 \text{ bubbles, leading to a } R_0 \text{ of } 4.9 / \sqrt[3]{34} = 3.1 \mu\text{m}$$

The values of bubble sizes obtained for the different t_{on} in Table 1 are best explained with 3.1 μm (i.e., one can retrieve them by considering coalescence of bubbles of initial R_0 3.1 μm).

In O₂ too, interactions between bubbles are already important for $t_{\text{on}} = 1$ ms. The smallest measured size is 3.5 μm , and an initial radius of 2.8 μm ($= 3.5 / \sqrt[3]{2}$) allows to interpret experimental values for the different t_{on} .

The nitrogen case is particular and very interesting because bubble size distributions are always very narrow – yet, an intense coalescence is observed: 2.2 μm can be obtained by the coalescence of 4 1.4- μm bubbles, 2.8 μm by that of 8 1.4- μm bubbles (or coalescence of 2 previously formed 2.2- μm bubbles). Also the smallest measured size, 1.4 μm , can be derived from coalescence of two 1.1- μm bubbles, or four 0.88- μm bubbles.

To try and shed light on the nitrogen case, it is useful to look at Ar-N₂ mixtures and at air, for which the SL intensity is high enough to allow measurements with $t_{\text{on}} = 1$ ms. Air is mainly composed of nitrogen (78%) and of oxygen (21%). Its behavior is thus expected to show similarities with these two gases. Values presented in Table 1 are much smaller than O₂ values and close to N₂ ones, as expected from air composition. However, it is noteworthy that they are smaller than pure N₂ ones, indicating a smaller extent of coalescence. The minimum measured value of 1.1 μm allows to explain the different radius values obtained: 1.4 μm would correspond to the coalescence of 2 bubbles, 1.7 μm to the equivalent coalescence of 4 bubbles, 2.5 μm to 12. Obviously a R_0 of 0.88 μm (if one assumes that 1.1 μm corresponds to a coalesced bubble) also allows to explain the different experimental radii.

Sizes derived in Ar-N₂ mixture for $t_{\text{on}} = 1$ ms (Table 2) confirm that N₂ R_0 is most probably 0.9 or 1.1 μm . As soon as some N₂ is present in Ar, bubble sizes strongly decrease. They further decrease with an increase in N₂ content, reaching 1.1 μm for 80% N₂.

3.3. R_0 and extent of coalescence

Table 3 summarizes the derived R_0 for different gases and the extent of coalescence at different t_{on} , i.e., the number of bubbles of equilibrium radius R_0 leading to the experimentally observed bubble sizes. Obviously, the real mechanism does not involve the coalescence of this (large) number of R_0 -bubbles in one single step, but successive coalescences of bubbles of growing size.

Let's first consider equilibrium radii and compare them with data from the literature. This comparison is deliberately restricted to multi-bubble studies since single-bubble measurements are usually performed in (at least partly) degassed solutions and the dissolved gas content is a

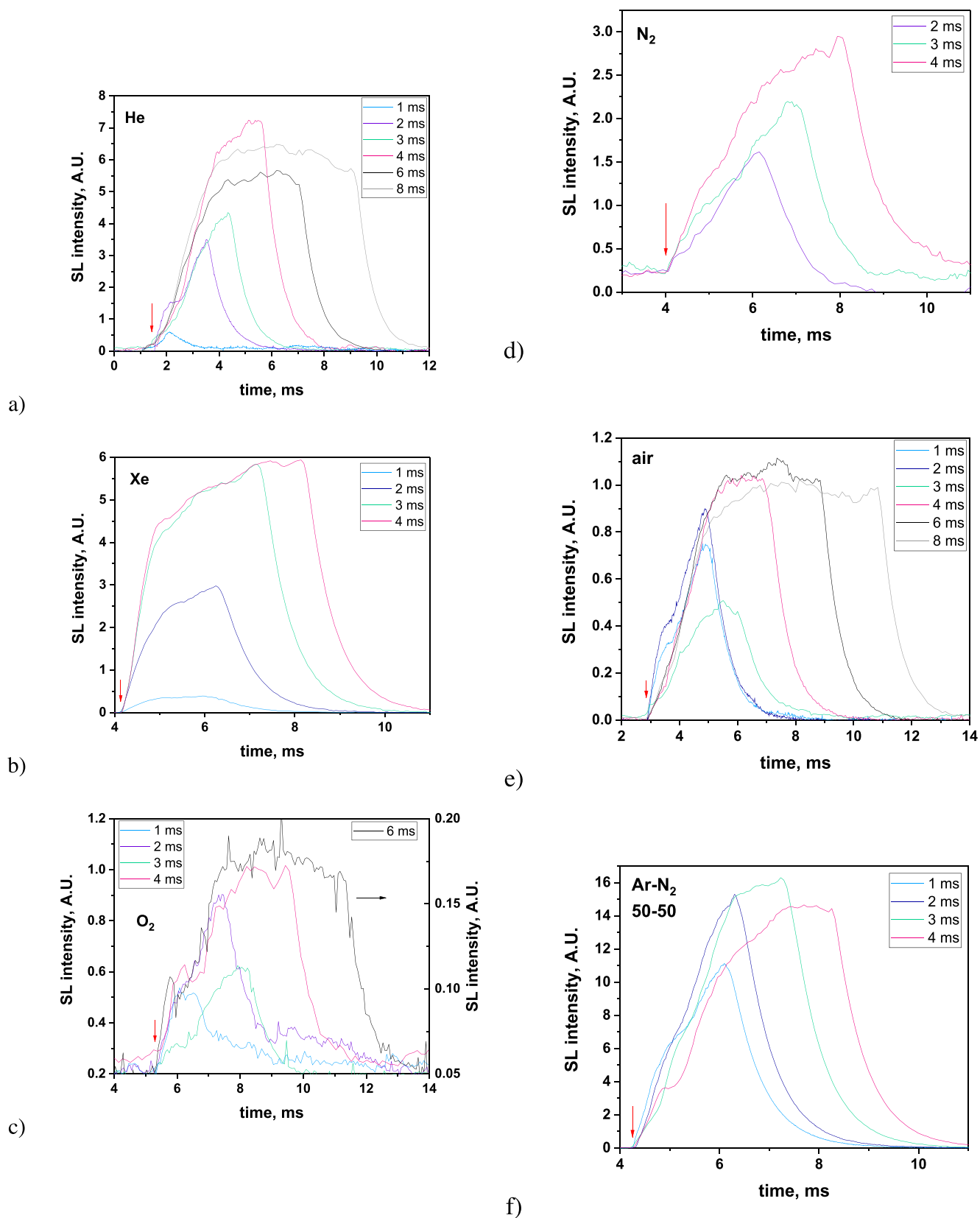


Fig. 1. Evolution of the SL intensity during t_{on} for different t_{on} for a) He ($V_{PMT} = 1000$ V), b) Xe ($V_{PMT} = 550$ V), c) O₂ ($V_{PMT} = 1000$ V (1–4 ms) or 650 V (6 ms)), d) N₂ ($V_{PMT} = 1000$ V), e) air ($V_{PMT} = 800$ V) and f) Ar-N₂ 50–50 ($V_{PMT} = 1000$ V). The red arrow indicates the beginning of t_{on} . (For interpretation of the references to colour in this figure legend, the reader is referred to the web version of this article.)

Table 1

Experimental bubble sizes (in μm) obtained from SL intensity vs. t_{off} plots for different gases and different t_{on} . Given sizes are $R_{\text{min}}\text{-}R_{\text{max}}/R_{\text{middle}}$, i.e. radii corresponding to the end, the beginning and the middle of the SL intensity increase in I_{SL} vs t_{off} plots, as previously [10] defined.

t_{on} , ms	Ar*	He	Xe	O ₂	N ₂	air	Ar-N ₂ 50–50
1	3.7–4.3 / 3.8	1.2–1.9 / 1.5	4.9–5.1 / 5.0	3.5–4.0 / 3.6	Too dim	1.1–1.4 / 1.2	1.5–1.8 / 1.7
2	3.9 – 4.7 / 4.0	1.8–2.6 / 1.9	5.2–6.1 / 5.9	3.6–4.9 / 3.9	1.4 / 1.4	1.1–1.3 / 1.2	1.6–2.1 / 1.8
3	3.7 – 4.3 / 4.0	2.8–4.1 / 3.3	6.0–7.8 / 7.0	4.1–5.0 / 4.7	2.2–2.4 / 2.2	1.7–1.8 / 1.8	2.7–2.9 / 2.8
4	3.1 – 4.9 / 4.7	3.1–3.3 / 3.2	7.8–8.6 / 8.2	5.3–7.2 / 6.2	2.8–2.8 / 2.8	2.5–2.7 / 2.6	2.9–3.8 / 3.7
6	5.3 – 6.2 / 6.1	5.3–6.5 / 5.8		6.5–8.3 / 7.6		3.1–3.4 / 3.3	
8	5.6 – 6.7 / 6.4	/ 5.9					

* From previous study [10].

Table 2

Experimental bubble sizes (in μm) obtained from SL intensity vs. t_{off} plots and estimated cavitation bubble size (R_0) for different N₂ contents in Ar at $t_{\text{on}} = 1$ ms.

% N ₂	$R_{\text{min}}\text{-}R_{\text{max}} / R_{\text{middle}}$, μm	R_0 , μm	Coalescence range
0	3.7–4.3 / 3.8	3.0	2–3
10	1.8–2.5 / 2.0	1.8	1–3
30	1.4–2.2 / 1.6	1.4	1–4
50	1.5–1.8 / 1.7	1.4	1–3
80	1.1–1.5 / 1.3	1.1	1–3
100	–	1.1 or 0.9	–

parameter that strongly affects the ambient radius [18]. Most experimental data correspond to low frequencies, between 20 kHz and 40 kHz, and to air-saturated water [19–22]. They report equilibrium radii generally in the range 1–6 μm . The most accurate study [22] underlines that although most observed bubbles have an equilibrium radius between 2 and 4 μm , this result is biased because values below 2.2 μm are not accessible to their experimental determination. What is more, they observed that the bubble size distribution increases when decreasing R_0 towards 2 μm . This pleads in favor of small active bubbles. This will be true at a high frequency, since the active bubble size is expected to decrease with the US frequency [23]. Experimental bubble equilibrium sizes determined by Labouret and Frohly at 350 kHz [5,6] support this result: they are in the range 2–3.5 μm but the authors state that many smaller bubbles are present (but bubbles smaller than 2 μm are not accessible to the measurement).

Using laser diffraction and pulsed sonication at 443 kHz under air, Iida et al. [24] observed an increase in size with the pulse length, due to bubble coalescence. When limiting it with SDS (5 mM) they derived a mean radius of 3.6 μm , but this radius is probably overestimated since sizes smaller than 2 μm were not accessible to the measurement.

Bubble sizes previously determined with the present technique were most of the time also impacted by coalescence, due to the too long t_{on} . For air-saturated water sonicated at 515 kHz ($t_{\text{on}} = 4$ ms) [9] sizes of 2.8–3.7 μm were obtained, that decreased to 0.9–1.7 μm in the presence of 1.5 mM SDS, in a good agreement with presently determined values. The bubble size was reported to depend on the pulse width [25] though this observation was not explained by coalescence but by bubbles in clusters experiencing different acoustic pressures and thus having different sizes: 2.5 μm for $t_{\text{on}} = 1$ ms, 3.8 μm for 4 ms. An extrapolation

Table 3

Considered R_0 and extent of coalescence (in number of equivalent R_0 -bubbles) for the different gases and t_{on} .

	Ar	He	Xe	O ₂	N ₂	air	Ar-N ₂ 50–50
Considered R_0 , μm	3.0	1.2	3.1	2.8	1.1 (or 0.9)	1.1 (or 0.9)	1.4
$t_{\text{on}} = 1$ ms	2–3	1–4	4–5	2–3	–	1–2 (2–4)	1–2
$t_{\text{on}} = 2$ ms	2–4	3–10	5–8	2–6	2 (4)	1–2 (2–4)	1–3
$t_{\text{on}} = 3$ ms	2–3	13–40	7–16	3–6	8–10 (16–20)	4–5 (8–10)	6–7
$t_{\text{on}} = 4$ ms	1–4	17–21	16–22	7–17	16 (32)	12–15 (24–30)	7–16
$t_{\text{on}} = 5$ ms	4–5	–	–	–	–	–	–
$t_{\text{on}} = 6$ ms	5–9	86–159	–	12–26	–	22–30 (44–60)	–
$t_{\text{on}} = 7$ ms	6–11	–	–	–	–	–	–
$t_{\text{on}} = 8$ ms	6–11	81–159	–	–	–	41–56 (82–112)	–

to 0 ms gave sizes of 1.2–1.8 μm , close to the present value.

Under Ar, the value of 5.8 μm was reported [25] for $t_{\text{on}} = 5.8$ ms and 515 kHz for pre-saturated water, and of 3.0 – 5.8 μm at 355 kHz, $t_{\text{on}} = 4$ ms and a continuous gas flow [17]. The smallest value obtained with a gas flow agrees well with the presently determined one. Others can be explained by coalescence. The same two studies report values under He: 4.1 μm under saturation [25] and 3.75–4.0 μm with a gas flow [17].

The only experimental value reported for Xe is at low frequency and in phosphoric acid [26]: maximum expansion radii are of ~ 50 –80 μm at 36.5 kHz, and of ~ 75 –240 μm at 23 kHz. Considering a factor of 10 between maximum expansion radii and equilibrium ones [27], these values correspond to equilibrium radii $R_0 \sim 5$ –8 and ~ 7.5 –24 μm . A high viscosity can be expected to decrease surface instabilities and thus allow bigger ambient radii. Considering the higher viscosity and the lower frequency, these results well agree with the present sizes.

Presently determined ambient radii also show agreement with calculated literature data. Yasui [28] calculated that SL bubbles had a R_0 in the range 0.3–8.0 μm for air-saturated water at 300 kHz. The single-bubble chemical model of Merouani indicated that bubbles with R_0 in the approximate range 4–6 μm (depending on the acoustic intensity) lead to a maximum in hydrogen production for Ar-saturated water at 355 kHz [29], while with O₂ and 300 kHz [30] the optimal sizes for oxidant production were around 4 μm for 1.5 bar and increasing with the acoustic pressure.

It is to be noted that the present values are quite close to the Blake threshold, especially for He, N₂ and air. For water (whose surface tension is 0.0725 N/m), it corresponds to 1 μm for an acoustic pressure of 1.5 bar, and to 0.5 μm at 3 bar. These values are expected to be independent from the gas nature, since interactions between water molecules and gas ones are negligible compared to those between water molecules in the liquid phase, so that the surface tension is essentially a constant for water.

Table 4 compares values of R_0 with physical properties of the gas. In general, it indicates that R_0 increases with the gas solubility, the gas density and the gas viscosity. It may appear surprising that very close R_0 are obtained for rare gases and molecular gases (He and N₂ on the one hand, Ar, O₂, Xe on the other hand), and also for some gases with very different solubilities (Ar and Xe). Obviously, the range of ambient radii leading to plasma formation and SL emission at collapse is the result of a complex interplay between several physical parameters. One may for instance assume that a stronger collapse, leading to a more efficient

Table 4

Considered R_0 , gas solubility [11], gas density, gas viscosity, speed of sound, diffusion coefficient [12–14] and ionization energy [15].

Gas	Ar	He	Xe	O ₂	N ₂	air	Ar-N ₂ 50–50
Considered R_0 , μm	3.0	1.2	3.1	2.8	1.1 (or 0.9)	1.1 (or 0.9)	1.4
Gas solubility, mol/L	1.48 10^{-3}	4.0 10^{-4}	7.2 10^{-3}	1.75 10^{-3}	8.57 10^{-4}		
Gas density in the bubble	1.73	0.167	5.67	1.38	1.21		
Gas viscosity, $\mu\text{Pa}\cdot\text{s}$	22.7	19.9	23.2	20.7	17.9		
Speed of sound in the gas, $\text{m}\cdot\text{s}^{-1}$	323	1017	178	330	353		
Gas diffusion coefficient, m^2/s	1.23 10^{-9}	6.76 10^{-9}	1.57 10^{-9}	1.54 10^{-9}	1.29 10^{-9}		
Ionization energy, eV	15.76	24.59	12.13	12.07	15.58		

energy concentration, would be necessary to form a plasma out of a gas with high ionization potential or subject to energy losses by dissociation, chemical reactions and vibrational/rotational excitation (i.e. a molecular gas). The gas viscosity may play a role in the bubble dynamics, the formation of surface instabilities and the symmetry of the collapse.

Considering rare gases, Ar and Xe show similar R_0 while He bubbles are much smaller. Smaller the bubble size, the more symmetrical is the collapse, thus the strongest it should be – which is necessary for He to form a plasma, due to its high ionization energy (Table 4). Besides, gas segregation [31] inside the collapsing bubbles and enhanced water condensation on the bubble wall at the end of the collapse in the He case may also decrease the necessary R_0 to reach a critical energy concentration. It is also to be noted, considering Ar and Xe, that a similar R_0 does not imply a similar radius at the maximum of bubble expansion, due to the very different gas solubilities (Xe bubbles will grow more).

This simplified approach allows to shed some first light on possible reasons leading to the experimentally determined R_0 for different gases. It however does not explain the particular case of nitrogen and Ar-N₂ mixtures where even a very low amount of N₂ leads to a strong decrease in R_0 . This example underlines that phenomena coming into play are complex, not limited to thermodynamics, and deserve detailed studies, such as on the influence of the gas nature on bubble deformation during collapse.

Concerning the extent of coalescence (Fig. 2), it also appears to result from the interplay of different physical phenomena: comparing Fig. 2 with Table 4 shows no direct correlation of the extent of coalescence with any of the listed properties. It also does not seem to be correlated with R_0 (Fig. 3). Considering only rare gases, where Ar shows the lowest coalescence, one may speculate that xenon's much higher solubility leads to a higher number of bubbles and consequently higher probability of coalescence, and that helium's very high diffusion coefficient may lead to more interactions between bubbles. Oxygen shows a behavior close to Ar, though with some tendency towards more coalescence. This similarity is in agreement with their close solubilities and bubble size. Nitrogen and air show similar ranges of coalescence, at least if the same R_0 is considered for both.

It is to be noted that the width of the coalescence range strongly depends on the gas nature, even for a similar mean equivalent number of bubbles of radius R_0 : for instance the interval is very large for He and very small for N₂. This fact, combined to the different evolutions of coalescence at larger t_{off} (Table 3), clearly confirms that several parameters play a role in this complex phenomenon: gas solubility, diffusion coefficient, bubble size, but also most probably the bubble dynamics, its deviation from sphericity and the extent of emission of

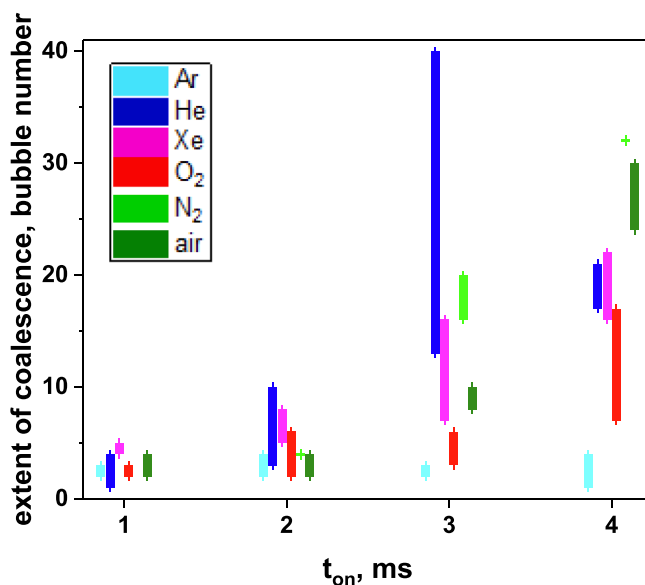


Fig. 2. Evolution of the extent of coalescence (in equivalent number of bubbles of radius R_0) with t_{on} for Ar, He, Xe, O₂, N₂ and air.

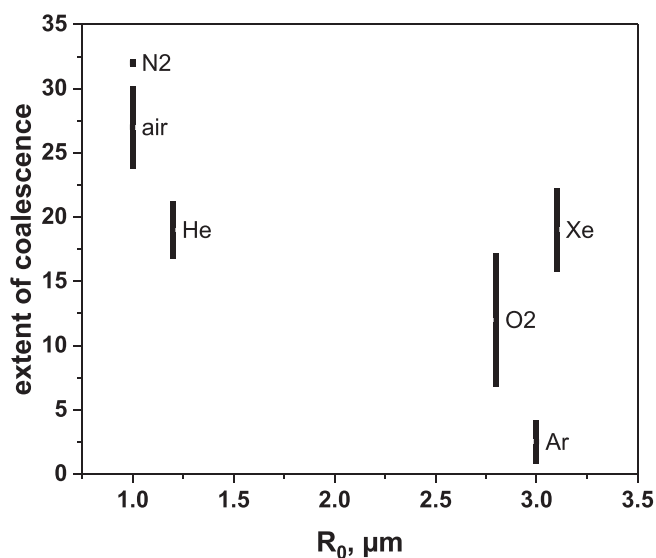


Fig. 3. Extent of coalescence (in equivalent number of bubbles of radius R_0) as a function of the estimated R_0 , for $t_{\text{on}} = 4$ ms.

daughter bubbles at collapse.

4. Conclusion

Using the recently developed approach [10] coupling pulsed US and SL intensity measurements for an interval of on-times, ambient radii could be evaluated for different gases: 3.0 μm for Ar, 1.2 μm for He, 3.1 μm for Xe, 2.8 μm for O₂, around 1 μm for N₂ and air. As previously observed on Ar, increasing the on-time leads to the determination of the size of coalesced bubbles. The extent of coalescence strongly depends on the gas nature. No single physical property of the gas allows to explaining it, but it seems to increase with the gas solubility, which is attributed to the formation of a larger number of bubbles, thus increasing the probability of interactions. Also a high gas diffusion coefficient appears to favor coalescence. A devoted theoretical modelling study would be needed. It would also be interesting to try and link present results with observations of the bubble dynamics and in

particular bubble deformation (surface instabilities) and emission of daughter bubbles at collapse.

Funding

This research did not receive any specific grant from funding agencies in the public, commercial, or not-for-profit sectors.

Declaration of Competing Interest

The authors declare that they have no known competing financial interests or personal relationships that could have appeared to influence the work reported in this paper.

References

- [1] F. Reuter, S. Lauterborn, R. Mettin, W. Lauterborn, Membrane cleaning with ultrasonically driven bubbles, *Ultrason. Sonochem.* 37 (2017) 542–560.
- [2] G. ter Haar, Therapeutic applications of ultrasound, *Prog. Biophys. Mol. Biol.* 93 (2007) 111–129.
- [3] S. Labouret, J. Frohly, Study in a UHF electromagnetic resonant cavity of a bubble field induced by ultrasonic cavitation, *Eur. Phys. J.-Appl. Phys.* 10 (2000) 231–237.
- [4] S. Labouret, J. Frohly, Bubble size distribution estimation via void rate dissipation in gas saturated liquid. Application to ultrasonic cavitation bubble fields, *Eur. Phys. J.-Appl. Phys.* 19 (2002) 39–54.
- [5] S. Labouret, J. Frohly, Size distribution of inertial bubbles in an 344 kHz ultrasonic cavitation field, in: *International Congress on Ultrasonics*, Vienna, 2007.
- [6] S. Labouret, J. Frohly, Distribution en tailles des bulles d'un champ de cavitation ultrasonore, in: *10ème Congrès Français d'Acoustique*, Lyon, France, 2010.
- [7] S.S. Xu, Y.J. Zong, X.D. Liu, M.X. Wan, Size Distribution Estimation of Cavitation Bubble Cloud via Bubbles Dissolution Using an Ultrasound Wide-Beam Method, in: J.B. Fowlkes, V.A. Salgaonkar (Eds.) *Proceedings from the 14th International Symposium on Therapeutic Ultrasound*, Amer Inst Physics, Melville, 2017.
- [8] A. Brothie, F. Grieser, M. Ashokkumar, Effect of power and frequency on bubble-size distributions in acoustic cavitation, *Phys. Rev. Lett.* 102 (8) (2009), <https://doi.org/10.1103/PhysRevLett.102.084302>.
- [9] J. Lee, M. Ashokkumar, S. Kentish, F. Grieser, Determination of the size distribution of sonoluminescence bubbles in a pulsed acoustic field, *J. Am. Chem. Soc.* 127 (2005) 16810–16811.
- [10] R. Pflieger, J. Bertolo, L. Gravier, S.I. Nikitenko, M. Ashokkumar, Impact of coalescence in the determination of bubble sizes using a pulsed US technique: Part 1 - Argon bubbles in water, submitted to, *Ultrason. Sonochem.* (2021), <https://www.engineeringtoolbox.com/gases-solubility-water-d-1148.html>, in.
- [11] B. Jahne, G. Heinz, W. Dietrich, Measurement of the diffusion-coefficients of sparingly soluble gases in water, *J. Geophys. Res.-Oceans* 92 (1987) 10767–10776.
- [12] D.M. Maharajh, J. Walkley, Temperature-dependence of diffusion-coefficients of Ar, CO₂, CH₄, CH₃Cl, CH₃Br, and CHCl₂F in water, *Can. J. Chem.-Revue Canadienne De Chimie* 51 (1973) 944–952.
- [13] <https://www.engineeringtoolbox.com/diffusion-coefficients-d-1404.html>, in.
- [14] NIST Atomic Spectra Database Ionization Energies Form, <https://physics.nist.gov/PhysRefData/ASD/ionEnergy.html>, in.
- [15] P.S. Epstein, M.S. Plesset, On the stability of gas bubbles in liquid-gas solutions, *J. Chem. Phys.* 18 (11) (1950) 1505–1509.
- [16] R. Pflieger, J. Lee, S.I. Nikitenko, M. Ashokkumar, Influence of He and Ar flow rates and NaCl concentration on the size distribution of bubbles generated by power ultrasound, *J. Phys. Chem. B* 119 (39) (2015) 12682–12688.
- [17] F.R. Young, *Sonoluminescence*, in, CRC Press, New York, 2005.
- [18] F. Burdin, N.A. Tsochatzidis, P. Guiraud, A.M. Wilhelm, H. Delmas, Characterisation of the acoustic cavitation cloud by two laser techniques, *Ultrason. Sonochem.* 6 (1-2) (1999) 43–51.
- [19] T. Niederdrank, B. Wiesand, The temperature dependent behaviour of a cavitation bubble field, *Acustica* 84 (1998) 425–431.
- [20] R. Mettin, S. Luther, W. Lauterborn, Bubble size distribution and structures in acoustic cavitation, in: *2nd Conf. on Applications of Power Ultrasound in Physical and Chemical Processing*, 1999, pp. 125–129.
- [21] F. Reuter, S. Lesnik, K. Ayaz-Bustami, G. Brenner, R. Mettin, Bubble size measurements in different acoustic cavitation structures: Filaments, clusters, and the acoustically cavitating jet, *Ultrason. Sonochem.* 55 (2019) 383–394.
- [22] K. Yasui, Influence of ultrasonic frequency on multibubble sonoluminescence, *J. Acoust. Soc. Am.* 112 (2002) 1405–1413.
- [23] Y. Iida, M. Ashokkumar, T. Tuziuti, T. Kozuka, K. Yasui, A. Towata, J. Lee, Bubble population phenomena in sonochemical reactor: I Estimation of bubble size distribution and its number density with pulsed sonication – laser diffraction method, *Ultrason. Sonochem.* 17 (2010) 473–479.
- [24] A. Brothie, T. Statham, M.F. Zhou, L. Dharmarathne, F. Grieser, M. Ashokkumar, Acoustic bubble sizes, coalescence, and sonochemical activity in aqueous electrolyte solutions saturated with different gases, *Langmuir* 26 (2010) 12690–12695.
- [25] C. Cairós, R. Mettin, Simultaneous high-speed recording of sonoluminescence and bubble dynamics in multibubble fields, *Phys. Rev. Lett.* 118 (6) (2017), <https://doi.org/10.1103/PhysRevLett.118.064301>.
- [26] R. Pflieger, S.I. Nikitenko, C. Cairós, R. Mettin, Characterization of Cavitation Bubbles & Sonoluminescence, Springer Nature, 2019.
- [27] K. Yasui, T. Tuziuti, J. Lee, T. Kozuka, A. Towata, Y. Iida, The range of ambient radius for an active bubble in sonoluminescence and sonochemical reactions, *J. Chem. Phys.* 128 (2008), 184705.
- [28] S. Merouani, O. Hamdaoui, The size of active bubbles for the production of hydrogen in sonochemical reaction field, *Ultrason. Sonochem.* 32 (2016) 320–327.
- [29] S. Merouani, O. Hamdaoui, Y. Rezgui, M. Guemini, Effects of ultrasound frequency and acoustic amplitude on the size of sonochemically active bubbles - Theoretical study, *Ultrason. Sonochem.* 20 (2013) 815–819.
- [30] K. Yasui, Segregation of vapor and gas in a sonoluminescing bubble, *Ultrasonics* 40 (2002) 643–647.